temperature gradient and horizontal mass flow, *Proc. Ninth Int. Heat Transfer Conf.*, Vol. 5, pp. 153–158. Hemisphere, Washington, DC (1990).
3. D. A. Nield, D. M. Manole and J. L. Lage, Convection induced by inclined thermal and solutal gradients in a shallow horizontal layer of a porous medium, *J. Fluid Mech.* **257,** 559–574 (1993).
4. J. E. Weber, Convection in a porous medium with horizontal and vertical gradients, *Int. J. Heat Mass Transfer* **17,** 241–248 (1974).
5. A. E. Gill, A proof that convection in a porous vertical slab is stable, *J. Fluid Mech.* **35,** 545–547 (1969).
6. B. Straughan, A nonlinear analysis of convection in a porous vertical slab, *Geophys. Astrophys. Fluid Dyn.* **42,** 269–276 (1988).
7. D. A. S. Rees, The stability of Prandtl–Darcy convection in a vertical porous layer, *Int. J. Heat Mass Transfer* **31,** 1529–1534 (1988).
8. J. G. Georgiadis and I. Catton, Free convective motion in an infinite vertical porous slot: the non-Darcian regime, *Int. J. Heat Mass Transfer* **28,** 563–572 (1985).
9. P. G. Daniels, P. A. Blythe and P. G. Simpkins, Thermally driven shallow flow in porous media: the intermediate regime, *Proc. R. Soc. Lond.* **A406,** 263–285 (1986).

Pergamon

Int. J. Heat Mass Transfer. Vol. 37, No. 18, pp. 3025–3030, 1994

0017–9310/94 $7.00 + 0.00

Comparison of convective heat transfer to perimeter and center jets in a confined, impinging array of axisymmetric air jets

AARON M. HUBER and RAYMOND VISKANTA†

Heat Transfer Laboratory, School of Mechanical Engineering, Purdue University, West Lafayette, IN 47907-1288, U.S.A.

(*Received* 27 *September* 1993 *and in final form* 12 *February* 1994)

INTRODUCTION

Heat transfer is enhanced through jet impingement for many different applications, including the tempering and shaping of glass, the annealing of metal and plastic sheets, the cooling of gas turbine blades, and the drying of textiles, veneer, paper, and film materials. However, a disadvantage of impingement heating or cooling can be the nonuniformity of the heat flux distribution. For large arrays the majority of jets will be center jets, i.e. surrounded on all sides by adjacent jets. However, for small arrays, a significant fraction of the impingement surface is covered by perimeter or boundary jets which are not completely surrounded by adjacent jets. For improved understanding of the flow and heat transfer in small arrays, the similarities and differences between the center jet and perimeter jets in a 3 by 3 square array ($X_n/D = 6.0$) were studied. Only limited local heat transfer coefficient data have been reported in the literature [1], and no known study examined the differences between a center and perimeter jet in a small array. Hence, local Nusselt numbers were obtained for $Re_D = 10\,200$ and 17 000 at $H/D = 6.0$, 1.0, and 0.25 with open spent air exits similar to the conditions used by Huber and Viskanta [2]. Symmetry was assumed and the convective coefficients were measured only over the lower quadrant shown in Fig. 1. This was done to keep the data files manageable in size.

The heat transfer coefficients were measured using a heated 0.025 mm thick stainless steel foil impingement surface coated with liquid crystals. The temperature distribution along the surface was determined by measuring the reflected wavelength of light from the liquid crystals with the use of bandpass filters and an electronic digitizer. With this technique local Nusselt number distributions are obtained that show the uniformity of coverage along the impingement surface. The experimental method and conditions are discussed in detail by Huber and Viskanta [2] and Huber [1].

RESULTS AND DISCUSSION

Local Nusselt numbers

The local Nusselt numbers are presented by contour and three-dimensional plots for the measurement area shown in Fig. 1. While experimental data were obtained for two Reynolds numbers, 10 200 and 17 000, the largest differences

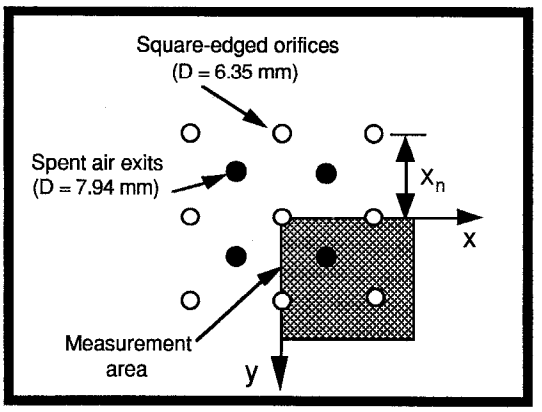

Fig. 1. Measurement area for perimeter jet experiments.

†Author to whom correspondence should be addressed.

NOMENCLATURE

D	jet diameter [m]
H	distance from jet exit to impingement surface [m]
k	thermal conductivity of air at jet exit [W m^{-1} K^{-1}]
Nu_D	Nusselt number based on jet diameter, hD/k
Re_D	Reynolds number based on jet diameter, $4M/(\pi D\mu)$
r	radial distance from stagnation point of jet [m]
X_n	spacing between jets in a square array [m] (see Fig. 1)
x	distance along impingement surface [m] (see Fig. 1)
y	distance along impingement surface [m] (see Fig. 1).

Greek symbol

μ	air viscosity at jet orifice exit [N s m^{-2}].

were seen with the 17 000 Reynolds number. Therefore, the discussion will focus on the heat transfer coefficient data for this Reynolds number. Three-dimensional surface plots and corresponding contour plots of the local Nusselt number over the impingement surface are shown in Figs. 2–4 for $H/D = 6.0$, 1.0 and 0.25, respectively. The center jet is in the upper left-hand corner with only a quarter of its unit cell shown. The corner jet is at the bottom right-hand corner of the plot, with its entire unit cell shown. The two side jets are located at the top right-hand corner and bottom left-hand corner with only half of their respective unit cells plotted.

The contour plots reveal some slight differences between the local Nusselt number distributions for each jet, which are not shown by the surface plots. While the center jet exhibits axisymmetric contours, the contours for the perimeter jets are slightly non-axisymmetric and resemble ovals at all three spacings. For all the perimeter jets the local Nusselt number decreases more rapidly on the side near the center jet. Because the jet is not opposed in the outward direction, more of the air flows outward than toward the center jet (a lower pressure exists in the outward direction). This results in a more rapid decrease in the local Nusselt numbers on the side near the center jet. In addition, the spent air exits located on the diagonals between the jet orifices minimize the formation of secondary stagnation regions where adjacent wall jets merge. This results in a smoother transition.

At $H/D = 6.0$ (Fig. 2) the local Nusselt number distributions shown in the surface plot [Fig. 2(a)] for each jet appear fairly similar. The maximum local Nusselt numbers are all located at the stagnation points. Figure 2(b) shows the contours of constant local Nusselt number. Only very small differences between the local Nusselt number distributions for each jet are discernible. The local minimum Nusselt number between the jets occurs at virtually the same location in the spent air exit, which is located at the geometrical center of the area between the jets.

The local Nusselt number distributions for $H/D = 1.0$ and $Re_D = 17\,000$ are shown in Fig. 3. In the surface plot, Fig. 3(a), both the inner and outer secondary rings in the local Nusselt number distribution [1, 2] are clearly depicted and no large differences are evident between the four jets. Close observation of the contour plot shown in Fig. 3(b) also depicts a difference which was not evident at $H/D = 6.0$. This difference is the location of the minimum local Nusselt number between the jets. The minimum local Nusselt number is no longer centered between the jets directly over the spent air exit but has shifted outward (from the center jet the shift was from $r/D = 4.24$ to about $r/D = 5.0$) toward the corner jet. The smaller separation distance increased the flow resistance. This raised the pressure at the center of the array and increased the flow resistance for the perimeter wall jets to flow toward the center jet. Therefore, more of the air from the perimeter jets flowed outward, which decreased the flow in the inward directed wall jets. Thus, the location of the minimum local Nusselt number was moved radially outward from the center jet. However, just as with the other differences, this 15% increase in radial distance for the location of the minimum local Nusselt number is relatively small.

Figure 4 shows the local Nusselt number distributions for $H/D = 0.25$ and $Re_D = 17\,000$. As with both the $H/D = 6.0$ and 1.0 surface plots [Figs. 2(a) and 3(a)] there are no large discernible differences between the jets in Fig. 4(a). It can be seen that the outer secondary ring for $H/D = 0.25$ is approximately the same order of magnitude as the inner secondary ring for all but the corner jet. The corner jet still has a larger (in magnitude) inner secondary ring similar to $H/D = 1.0$. Apparently, the transition to turbulent flow in the wall jet boundary layer is not as sudden for the corner jet as for the other jets. This could be due to the smaller adjacent jet interference experienced by the corner jet.

Figure 4(b) depicts the contours of constant local Nusselt numbers for $H/D = 0.25$. As with Fig. 3(b), the location of the minimum local Nusselt number has shifted radially outward from the center jet. This shift is comparable to the shift seen at the 1.0 separation distance (from $r/D = 4.24$ to about 5.0). Also, while the secondary rings for $H/D = 0.25$ are larger in magnitude than those for $H/D = 1.0$, the minimum local Nusselt number located between the jets is smaller (36 compared to 28). This is because, for $H/D = 0.25$, the local Nusselt numbers decrease more rapidly in the wall jet region than for $H/D = 1.0$ [2]. Similar to the contour plots for the other two spacings, the contours of constant local Nusselt numbers for the perimeter jets are slightly oval in shape and not completely axisymmetric. However, it must be remarked again that the observed differences between the individual jets in the array are of the order of 10% which is the comparable to the experimental uncertainty.

Average Nusselt numbers

The local Nusselt number distributions were area averaged for each jet. The surface area over which average Nusselt numbers for each jet were obtained was a square with sides of length $X_n = 6D$. Only the corner jet had its entire open area unit cell included in the measurement area (Fig. 1). The side jets had only half of their unit cells in the measurement area, while the center jet had one quarter of its unit cell included. Assuming symmetry, the average Nusselt number for these partial unit cells was considered to be representative of the average Nusselt number for the entire unit cell. The larger measurement area (lower resolution of pixels) and symmetry assumption slightly increased the spatial uncertainty in the experimental measurements compared to the center jet unit cell measurements reported in Huber and Viskanta [2]. Therefore, the maximum uncertainty in the Nusselt number was about 9%. The average Nusselt numbers for each jet, corrected for heat losses and the small variations in the Reynolds number, are presented in Table 1. The value given for the entire array was determined by area averaging over the entire measurement surface area (Fig. 1) and

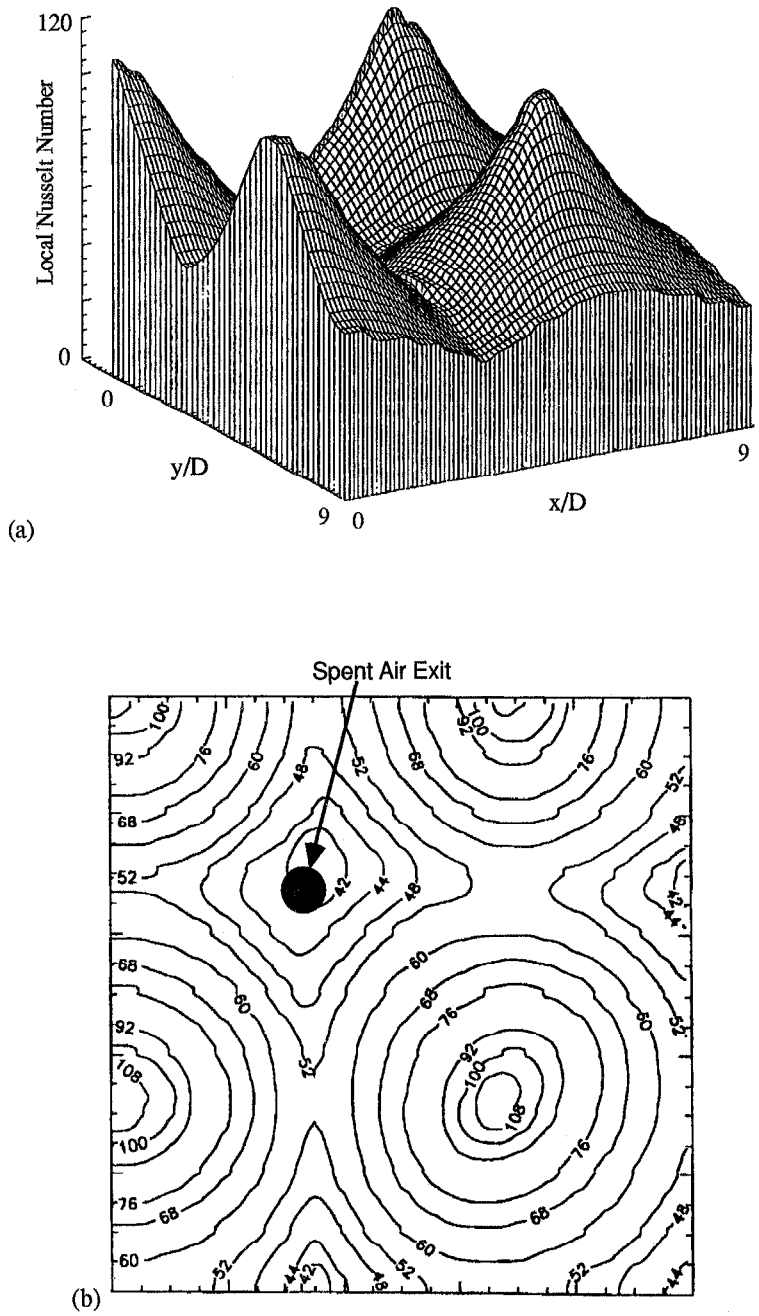

Fig. 2. Local Nusselt numbers for $H/D = 6.0$, $X_n/D = 6$, and $Re_D = 17\ 000$: (a) surface plot, and (b) contour plot (center jet at upper left-hand corner).

assuming symmetry for the other three quadrants of the array.

Comparison of the average Nusselt numbers for each jet indicates some interesting trends. Most important is the fact that there is a less than 12% difference between any of the average Nusselt numbers at a given separation distance. At $H/D = 6.0$ there is only a very small difference between the average Nusselt numbers. Because the corner jet experienced the least adjacent jet interference before impingement, it was expected that the average Nusselt number would be largest for the corner jet followed by the values for the side jets. The smallest average Nusselt number was expected to occur for the center jet, which would experience the largest amount of adjacent jet interference. This trend was observed with the experimental data shown in Table 1, but the differences between the values are small (1% or less) and within the range of experimental uncertainty.

As the separation distance was decreased the adjacent jet interference before impingement was minimized. Thus, the average Nusselt numbers significantly increased for the sep-

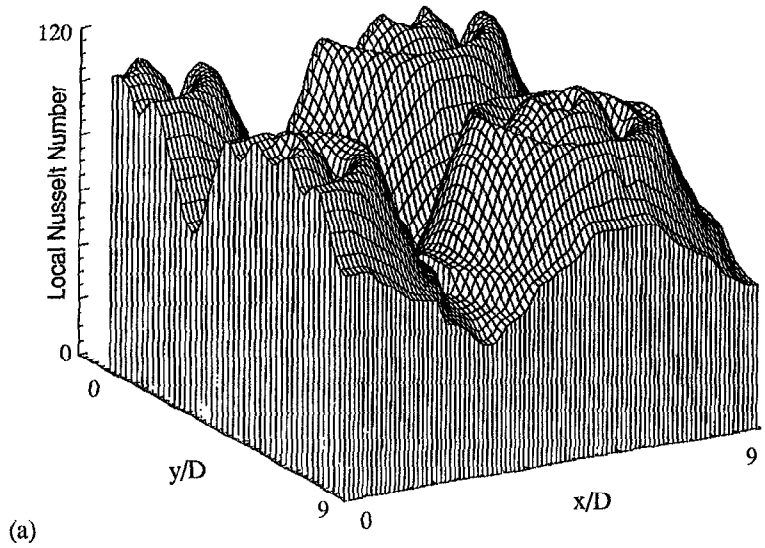

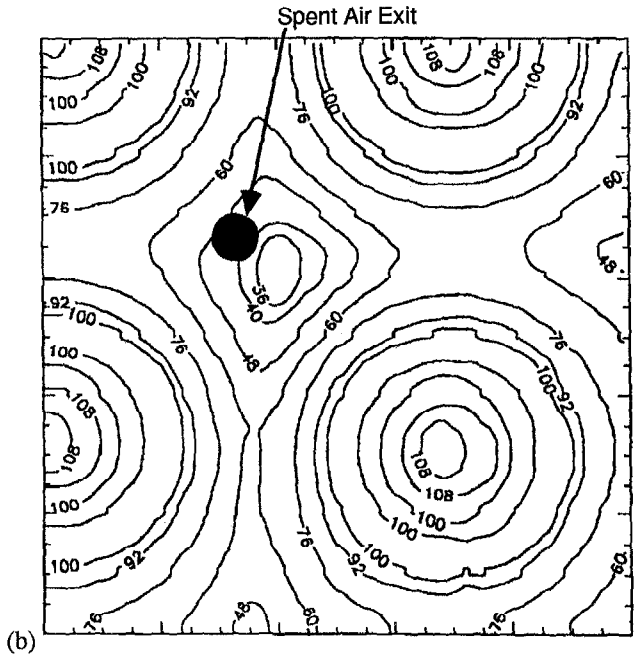

Fig. 3. Local Nusselt numbers for $H/D = 1.0$, $X_n/D = 6$, and $Re_D = 17\ 000$: (a) surface plot, and (b) contour plot (center jet at upper left-hand corner).

aration distances below $H/D = 6.0$. At $H/D = 1.0$ the trend seen at $H/D = 6.0$ was reversed with the center jet now possessing the largest average Nusselt number followed by the side jets and then the corner jet. This was due to the shift in the minimum local Nusselt number radially outward from the center jet and slight distortion of the symmetry for the perimeter jets as mentioned when discussing the local Nusselt number distributions. These same trends were evident with the smallest distance of $H/D = 0.25$, with larger differences occurring between the different perimeter and center jets.

In addition, the average values for the entire array are significantly lower for $H/D = 6.0$ than $H/D = 1.0$ and 0.25. This trend was also observed by other investigators [2–5]. Moreover, the average Nusselt number for the entire array is slightly higher for $H/D = 1.0$ than for $H/D = 0.25$. This trend was not observed with the center jet data [2] and is attributed to the corner jet which accounts for 44.4% of the total area. Ichimiya and Okuyama [3] observed a similar decrease in the average Nusselt number with a 2 by 2 square array as the separation distance was decreased below one jet

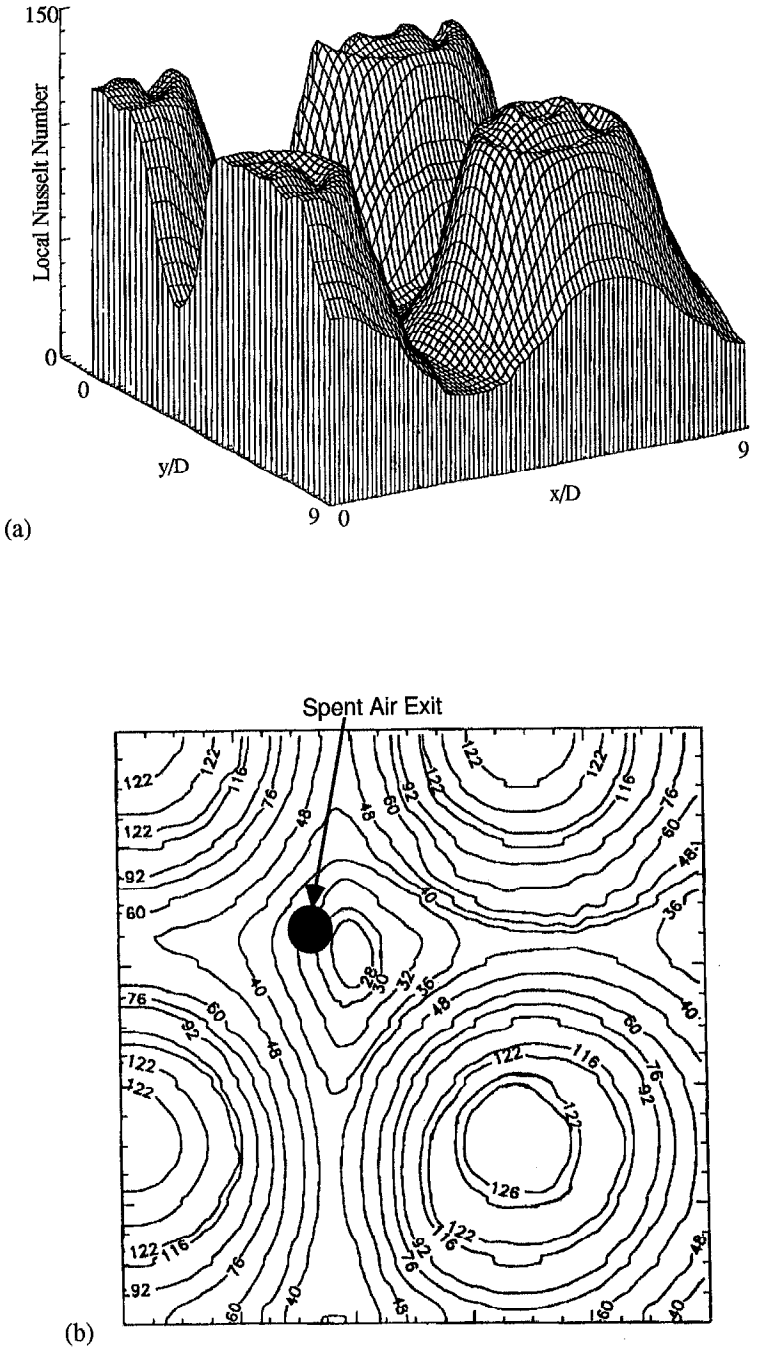

Fig. 4. Local Nusselt numbers for $H/D = 0.25$, $X_n/D = 6$, and $Re_D = 17\ 000$: (a) surface plot, and (b) contour plot (center jet at upper left-hand corner).

diameter. As seen with the local Nusselt number distributions, the corner jet at $H/D = 0.25$ did not have as pronounced an outer secondary ring as the other jets, and the magnitude of the secondary rings for the corner jet were similar to those observed at $H/D = 1.0$. Thus, the heat transfer enhancement of the outer secondary ring evident at $H/D = 0.25$ with the center and side jets was not seen with the corner jet. This resulted in a smaller average Nusselt number for the corner jet and entire array at $H/D = 0.25$ than at $H/D = 1.0$.

CONCLUSIONS

Differences between the local Nusselt number distributions for the center jet and perimeter jets were observed with the three-dimensional and contour plots. The wall jets for the perimeter orifices appeared to be stronger in the outward direction where there was no resistance from surrounding orifices. This is because the perimeter jets were not opposed on all sides like the center jet. Thus, the constant Nusselt number contours for the perimeter jets were more oval in

Table 1. Area average Nusselt numbers for open area unit cell and $Re_D = 17\,000$

H/D	Center jet	Side jet	Corner jet	Entire array
6.0	62.3	62.7	63.0	62.8
1.0	83.8	80.6	76.9	79.2
0.25	84.6	78.3	74.2	77.1

shape than circular. However, the differences between the contours for the center and perimeter jets were not large (about 15%). The small differences resulted in small variations of less than 12% between the average Nusselt numbers for the center and perimeter jets. The expected trends in the average Nusselt number between the jets were observed, but with small variations. Therefore, perimeter jets do differ from center jets, but for the conditions studied the differences are small.

REFERENCES

1. A. M. Huber, Heat transfer with impinging gaseous jet systems, Ph.D. Thesis, Purdue University, West Lafayette, IN (1993).
2. A. M. Huber and R. Viskanta, Effect of jet-to-jet spacing on convective heat transfer to confined, impinging arrays of axisymmetric air jets, *Int. J. Heat Mass Transfer* **37,** 2859–2869 (1994).
3. K. Ichimiya and K. Okuyama, Characteristics of impingement heat transfer caused by circular jets with confined wall. In *Proceedings of 3rd International Cold Regions Heat Transfer Conference* (Edited by J. P. Zarling), pp. 523–532. University of Alaska—Fairbanks, Fairbanks, AL (1991).
4. D. E. Metzger, T. Yamashita and C. W. Jenkins, Improvement cooling of concave surfaces with lines of circular air jets, *J. Engng Power* **91,** 149–158 (1969).
5. P. Hrycak, Heat transfer from a row of impinging jets to concave cylindrical surfaces, *Int. J. Heat Mass Transfer* **24,** 407–418 (1981).

Pergamon

Int. J. Heat Mass Transfer. Vol. 37, No. 18, pp. 3030–3033, 1994

0017-9310/94 $7.00+0.00

An investigation of a wave of temperature difference between solid and fluid phases in a porous packed bed

A. V. KUZNETSOV†

Mechanical Engineering Research Institute of Russian Academy of Sciences, 101830 Moscow, Russia

(*Received* 16 *December* 1993)

INTRODUCTION

Non-thermal equilibrium flow of a fluid through a porous bed is a subject of permanent interest for analytical and numerical investigations. Most of analytical studies of the phenomenon were concentrated on the Schumann model of a packed bed, obtained in ref. [1]. The model ignores the conduction terms in the solid and gas (liquid) phase energy equations. Originally the thermal capacity term in the fluid phase energy equation was also neglected, but in some further studies the effect of the thermal capacity of the fluid was included in the analysis. Analytical solutions for the model for various input conditions have been obtained in refs. [2–5]. Analysis and comparison of analytical solutions for the two-phase model (two energy equations) and the single-phase model (local thermal equilibrium assumption, and, as a result, one energy equation) are presented in ref. [6]. In refs. [7–9] a very general set of volume-averaged governing equations for non-thermal equilibrium condensing forced flow through a latent heat storage porous bed was presented and comprehensive numerical investigations of the phenomenon were carried out.

Distinguished from the previous analytical investigations the present analysis is based on solution by the perturbation technique of the full energy equations for fluid and solid phases, without neglecting any terms in the equations.

STATEMENT OF THE PROBLEM

Assumptions made in the analysis are outlined in the following:

(1) heat transfer is one-dimensional;
(2) thermal, physical, and transport properties are constant; and
(3) fluid phase is incompressible and mass flow rate at every cross-section of packed bed is constant.

Under the assumptions the set of governing equations presented in refs. [7–9] can be reduced to two energy equations for fluid and solid phases:

$$\Pi\rho_f c_f \frac{\partial T_f}{\partial t} + \rho_f c_f v \frac{\partial T_f}{\partial x} = \lambda_{feff} \frac{\partial^2 T_f}{\partial x^2} + h_{sf} a_{sf} [T_s - T_f], \quad (1)$$

$$(1-\Pi)\rho_s c_s \frac{\partial T_s}{\partial t} = \lambda_{seff} \frac{\partial^2 T_s}{\partial x^2} - h_{sf} a_{sf} [T_s - T_f], \quad (2)$$

where for the sake of simplicity we write $T_f = \langle T_f \rangle^f$, $T_s = \langle T_s \rangle^s$, $\rho_f = \langle \rho_f \rangle^f$, $\rho_s = \langle \rho_s \rangle^s$, $c_f = (c_p)_f$, $c_s = (c_p)_s$,

† Present address: Department of Mechanical Engineering, The Ohio State University, Columbus, OH 43210, U.S.A.